Robotica: decoupled elastostatic stiffness modeling of hybrid robots

Baoyu Wang[1] , Peixing Li[2], Chao Yang[3] , Xudong Hu[1] and Yanzheng Zhao[4]

[1]School of Mechanical Engineering, Zhejiang Sci-Tech University, Hangzhou, China
[2]School of Mechanical and Automotive Engineering, Shanghai University of Engineering Science, Shanghai, China
[3]College of Mechanical and Electrical Engineering, Jiaxing University, Jiaxing, China
[4]Research Institute of Robotics, Shanghai Jiao Tong University, Shanghai, China
Corresponding authors: Xudong Hu; Email: xdhu@zstu.edu.cn, Yanzheng Zhao; Email: yzh-zhao@sjtu.edu.cn

Abstract

A decoupling method is proposed for the elastic stiffness modeling of hybrid robots based on the rigidity principle, screw theory, strain energy, and Castigliano's second theorem. It enables the decoupling of parallel and serial modules, as well as the individual contributions of each elastic component to the mechanism's stiffness performance. The method is implemented as follows: (1) formulate limb constraint wrenches and corresponding limb stiffness matrix based on the screw theory and strain energy, (2) formulate the overall stiffness matrix of parallel and serial modules corresponding to end of the hybrid robots based on the rigidity principle, principle of virtual work, the wrench transfer formula, and strain energy methods, and (3) obtain and decouple the overall stiffness matrix and deflection of the robot based on the Castigliano's second theorem. Finally, A planar hybrid structure and the 4SRRR + 6R hybrid robot are used as illustrative examples to implement the proposed method. The results indicate that selectively enhancing the stiffness performance of the mechanism is the most effective approach.

1. Introduction

High-end manufacturing fields such as ships and port machinery have developed rapidly in recent years, and the demand for on-site welding and polishing of large-scale complex structural components has increased sharply. Traditional industrial robots are difficult to adapt to the work requirements of complex constructive components on the spot, and the on-site work of large-scale complex structural components is mainly completed by the workers' handmade operations. There are problems such as a harsh working environment and great labor intensity of workers during the working process. Therefore, the development of a wall-climbing robot that meets the demands of large-scale, complex structural on-site work holds significant practical importance and broad application prospects. The wall-climbing robot is generally designed as a hybrid robot, which consists of two parts of the wall-climbing parallel mechanism (PM) and serial module. The accuracy of the operation requires high rigidity. Establishing the correct stiffness model is the basis for conducting dynamic analysis. Wu [1–3] established the stiffness model of PMs and explored new methods for evaluating their dynamic performance. The establishment of a static elastic stiffness model analyzed by the robot is of great significance for evaluating stiffness performance at the predesign stage of the robot.

Analytical methods can establish the required analytical expression between the external wrench and the corresponding deflection. Analytical methods fall into four categories: the virtual joint method (VJM), the screw theory method, the strain energy method, and the matrix structure analysis (MSA) method.

The VJM treats each link as a rigid link supported by springs with six degrees of freedom (DOFs) at both ends. Zhang [4] established an elastostatic stiffness model of the Exechon overconstrained PMs using the VJM. Shen [5] established the stiffness model of the 2T1R PMs using the VJM. Kim [6] established stiffness models of the Tricept and 3-PRRR PMs by considering the flexibility of their links. However, the VJM may have redundant springs in certain directions, which requires combining sufficient number of deformation coordination equations to deal with these redundant spring constraints, makes the calculation process cumbersome; additionally, the VJM cannot obtain the compliance contribution matrix (CCM) and the elastic deflection contribution (EDC) for each elastic component in the robot [7, 8].

The screw theory method determines the constraint wrenches of the limb based on the screw theory, reducing the dimensions of the constraint wrenches imposed by each limb on the moving platform. This significantly reduces the required number of deformation coordination equations. Huang and Hu et al. [9, 10] established stiffness models of 4-R(CRR), 3-UPU, and 3-RPS PMs based on screw theory. They obtained the limb stiffness using the principle of superposition of deformations. Zhao [11–14] introduced the concept of limb constraint wrench stiffness matrices, and they analyzed overconstrained PMs such as 3-PRRR and 7-SS. However, the solution for limb stiffness matrices involves two projections, which makes the process somewhat cumbersome. Additionally, the CCM and EDC of each elastic member were not decoupled in the proposed modeling.

The strain energy method analyzes the strain energy of each elastic element and the entire mechanism based on material mechanics. It combines with the Castigliano's theorem to establish the overall stiffness matrix of the mechanism. This method has a clear physical interpretation and is computationally straightforward. Rezaei and Yan [15–18] established stiffness models for 3-PSP, 3-RRP, 2PRR-PPR, and delta PMs using the strain energy method. However, they only analyzed constrained PMs. Yang [19–21] later developed their work and applied the strain energy method to overconstrained PMs to establish stiffness models for the 2UPR-RPU and 2PUR-PSR PMs. However, these models only analyze PMs and do not consider hybrid mechanisms. They also do not decouple the contribution of each elastic component to the small end deformation of hybrid robots.

The MSA method considers each link as a standard beam element and combines sufficient number of deformation coordination equations to assemble the overall stiffness matrix. The MSA method achieves a good balance between calculation accuracy and calculation time. Klimchik [22, 23] presented a detailed process for the MSA method and established a stiffness model of the NaVaRo robot. Zhao [24] established the stiffness model for n(3RR1S) robot based on the MSA method and the screw theory. Yu [25] obtained the overall stiffness matrix for a 3-DOF PM and Cammarata [26] established stiffness models of both a spherical parallel robot and a Ragnar robot by combining the MSA method with condensation techniques. However, the MSA method involves high-dimensional matrices for multibody systems [27–29], and the research based on the MSA method mentioned above did not obtain the CCM and EDC for each elastic component.

The previous studies primarily focused on establishing the overall matrix of the mechanism, with limited exploration of the contributions of each component to the overall stiffness performance of the mechanism. Therefore, this paper places emphasis on studying the contributions of each elastic component to the overall stiffness performance of the mechanism. This focus provides a theoretical foundation for the effective improvement of the mechanism's stiffness performance.

The main contributions of this paper are as follows: (1) A decoupling method for the elastostatic stiffness model of hybrid robots is introduced. It is based on the rigidity principle, screw theory, strain energy, and Castigliano's second theorem. This method derives analytical expressions for the decoupled static stiffness model of hybrid robots and is applicable to both constrained and overconstrained hybrid robots. (2) The CCM of each elastic component of the hybrid robot is obtained based on the strain energy and Castigliano's theorem. (3) The linear and angular deflection contributions of each elastic component to the hybrid robots are decoupled to allow the contribution of each elastic component to the linear and angular stiffness performances of the hybrid robots to be evaluated quantitatively, thus providing a new approach for effective improvement of the linear/angular stiffness performances of the hybrid robots.
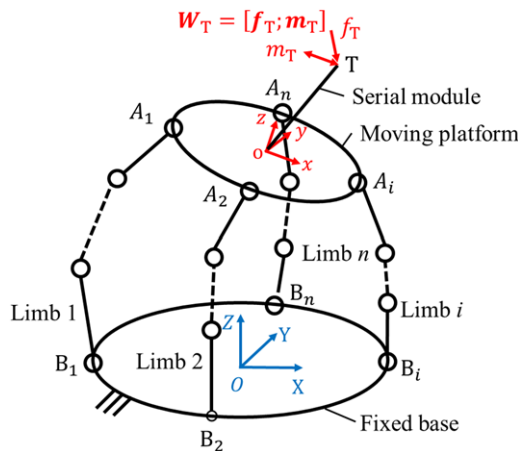
Figure 1. *Schematic diagram of a general hybrid robot.*

This paper is organized as follows. In Section 2, the decoupled elastostatic stiffness model based on the rigidity principle, screw theory, strain energy, and Castigliano's second theorem is proposed. In Section 3, a 3SPR + 1R hybrid mechanism is used as an example to demonstrate the procedure of the proposed method. In Section 4, the elastostatic model of the 4SRRR-6R hybrid robot is presented. Finally, in Section 5, conclusions are drawn from the work presented.

2. Unified stiffness model of hybrid robots based on the screw theory

The following assumptions are made for the hybrid robots:

1. The weights of all components are negligible.
2. The motors, moving platform, and all joints are rigid.
3. All joints are considered to be frictionless.
4. The links are considered to be flexible and the spatial composite deformation of the links, including the tension (or compression), shear, torsional and bending deformation components, is considered.
5. The deformation of all components is linear and within the elastic range.

Figure 1 shows a general model of a hybrid robot consisting of parallel and serial modules without loss of generality. The parallel module consists of a moving platform connected to a fixed platform by n limbs. The serial module is fixed at point o on the moving platform. *O-XYZ* and *o-xyz* denote the fixed coordinate frame and the moving coordinate frame, respectively. $\mathbf{W}_T = [\mathbf{f}_T; \mathbf{m}_T]$ is the external wrench exerted on the hybrid robot end, where $\mathbf{f}_T = [f_{Tx}, f_{Ty}, f_{Tz}]^T$; $\mathbf{m}_T = [m_{Tx}, m_{Ty}, m_{Tz}]^T$ denote the external force and moment, respectively.

The theoretical model used in the work is based on the rigidity principle, screw theory, strain energy, Castigliano's second theorem, and deformation compatibility equations (DCEs). Figure 2 shows the modeling process. The procedure of the proposed model in this paper is as follows: 1) According to the principle of superposition of deformation, the contribution of the hybrid robot to end deformation is equal to the superposition of the parallel and serial modules on end deformation. 2) Based on the rigidity principle, the contribution of the serial (parallel) module to end deformation can be obtained while the parallel (serial) module is considered to be rigid. 3) Decouple the total strain energy stored in the PM into the sum of the strain energy stored by each component (expressed based on external
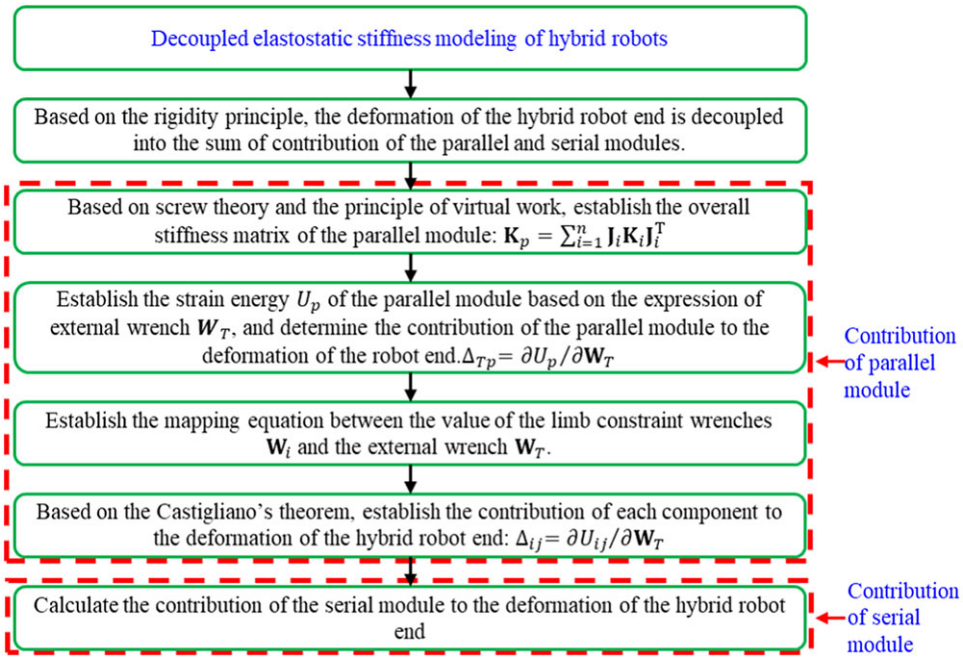
Figure 2. *Decoupled elastostatic stiffness modeling of hybrid robots.*

loads) $U = \sum_{i=1} \sum_{j=1} U_{ij}(\mathbf{W}_T)$. 4) Based on the Castigliano's second theorem, the contribution of each component to the end deformation of the hybrid robot can be obtained $\mathbf{\Delta}_{ij} = \partial U_{ij}/\partial \mathbf{W}_T$. The detailed steps are as follows:

2.1. Elastic deformation of hybrid robot end caused by parallel module
2.1.1 The contribution to the robot end deformation of the parallel module
Based on the rigidity principle, the contribution of the parallel module to end deformation can be obtained while the serial module is considered to be rigid.

According to the wrench transfer formula, the wrench acting on the point o of the parallel module can be expressed as follows:

$$\mathbf{W}_o = \begin{bmatrix} \mathbf{E}_3 & \mathbf{0}_3 \\ [\mathbf{S}_{oT} \times] & \mathbf{E}_3 \end{bmatrix} \mathbf{W}_T = \mathbf{D}_{To} \mathbf{W}_T = [\mathbf{f}_o; \mathbf{m}_o] \tag{1}$$

where $\mathbf{D}_{To}$ denotes the mapping matrix from $\mathbf{W}_T$ to $\mathbf{W}_o$. $[\mathbf{S}_{oT} \times]$ denotes the skew-symmetric matrix of vector $\mathbf{S}_{oT}$.

The DCEs between limb end and the attachment point o of the moving platform of the parallel module can be obtained [19] according to the principle of virtual work:

$$\mathbf{\Delta}_i = \mathbf{J}_i^T \mathbf{\Delta}_o \ (i = 1, 2, \cdots, n) \tag{2}$$

where $\mathbf{\Delta}_i$ denote the elastic deformation of the ith limb; $\mathbf{J}_i$ denote the unit constraint wrench system of the ith limb; and $\mathbf{\Delta}_o$ denotes the elastic deflection of the attachment point o of the moving platform.

The following equation can be obtained according to DCEs and the equilibrium equation of the spatial force system [19].

$$\mathbf{W}_o = \sum_{i=1}^{n} \mathbf{J}_i \mathbf{K}_i \mathbf{J}_i^T \mathbf{\Delta}_o = \mathbf{K}_p \mathbf{\Delta}_o \tag{3}$$
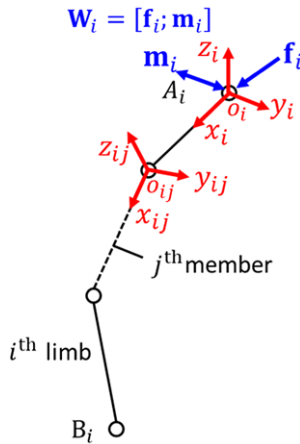
Figure 3. *General model of limb.*

where $\mathbf{K}_p$ denotes the overall stiffness matrix corresponding to the attachment point o of the moving platform of the parallel module.

Therefore, the elastic deflection of the attachment point of the moving platform under $\mathbf{W}_o$ is

$$\mathbf{\Delta}_o = \mathbf{K}_p^{-1}\mathbf{W}_o = \mathbf{C}_p\mathbf{W}_o \tag{4}$$

where $\mathbf{C}_p$ denotes the overall flexibility matrix corresponding to attachment point o of the moving platform of the parallel module.

The hybrid-robot terminal elastic deflection caused by parallel module under the assumption that the serial module to be rigid can be obtained as follows.

$$\mathbf{\Delta}_{Tp} = \begin{bmatrix} \mathbf{E}_3 & [\mathbf{S}_{To}\times] \\ \mathbf{0}_3 & \mathbf{E}_3 \end{bmatrix} \mathbf{\Delta}_o = \mathbf{T}_{To}\mathbf{\Delta}_o \tag{5}$$

where $\mathbf{E}_3$ and $\mathbf{0}_3$ denote the 3×3 identity matrix and zero matrix, respectively, $[\mathbf{S}_{To}\times]$ denotes the skew-symmetric matrix of vector $\mathbf{S}_{To,\text{ and }}$ $\mathbf{T}_{To}$ denotes the mapping matrix from $\mathbf{\Delta}_o$ to $\mathbf{\Delta}_{Tp}$.

From the analysis above, it is evident that to determine the contribution of the parallel module to the elastic deformation of the hybrid robot end, it is necessary to first calculate the overall stiffness matrix of the parallel module. The process for calculating the limb stiffness matrix and overall stiffness matrix of the parallel module can refer to [19].

Figure 3 presents a general model of the limb. $o_{ij}\text{-}\mathbf{x}_{ij}\mathbf{y}_{ij}\mathbf{z}_{ij}$ denotes the coordinate frame of jth member of ith limb, and axis $\mathbf{x}_{ij}$ is aligned with the direction of the limb member here.

Unit constraint wrench system $\mathbf{J}_i = [\$_{i1}^r, \$_{i2}^r, \$_{i3}^r]$ of the ith limb can be established based on the reciprocal screw theory, where $\$_{ij}^r = [\mathbf{r}_{ij}^r, \mathbf{r}_{oij}^r \times \mathbf{r}_{ij}^r]$ is the jth unit constraint wrench of the ith limb, $\mathbf{r}_{ij}^r$ is a unit vector pointing along the direction of the screw axis, and $\mathbf{r}_{oij}^r$ is the position of any point on the screw axis, with a magnitude of $\mathbf{W}_i = [\mathbf{f}_i; \mathbf{m}_i]$. $\mathbf{f}_i$ and $\mathbf{m}_i$ denote constraint force and moment, respectively.

Based on screw theory and the principle of virtual work, the overall stiffness matrix of the parallel module can be established:

$$\mathbf{K}_p = \sum_{i=1}^n \mathbf{J}_i\mathbf{K}_i\mathbf{J}_i^T \tag{6}$$

where $\mathbf{K}_i$ denotes the stiffness matrix of the ith limb corresponding to $\mathbf{W}_i$.

2.1.2 The contribution to the robot end deformation of each component

Elastic deformation $\boldsymbol{\Delta}_{ij}$ of the ith limb's j^{th} member corresponding to $\mathbf{W}_i$ can be obtained as follows according to Castigliano's second theorem:

$$\boldsymbol{\Delta}_{ij} = \frac{\partial U_{ij}}{\partial \mathbf{W}_i} = \mathbf{C}_{ij}\mathbf{W}_i \tag{7}$$

where U_{ij} denotes the strain energy of the ith limb's j^{th} member; $\mathbf{C}_{ij}$ denotes the flexibility matrix of the ith limb's j^{th} member corresponding to $\mathbf{W}_i$.

The strain energy of the ith limb's j^{th} member is given as

$$U_{ij} = \int_0^{L_{ij}} \left(\frac{f_{ijx}^2}{2E_{ij}A_{ij}} + \frac{f_{ijy}^2}{2G_{ij}A_{ijy}} + \frac{f_{ijz}^2}{2G_{ij}A_{ijz}} + \frac{m_{ijx}^2}{2G_{ij}I_{ijp}} + \frac{m_{ijy}^2}{2E_{ij}I_{ijy}} + \frac{m_{ijz}^2}{2E_{ij}I_{ijz}} \right) dv_{ij} \tag{8}$$

where $\mathbf{f}_{ij} = [f_{ijx}\, f_{ijy}\, f_{ijz}]^{\text{T}}$, $\mathbf{m}_{ij} = [m_{ijx}\, m_{ijy}\, m_{ijz}]^{\text{T}}$ denotes the internal force of the ith limb's j^{th} member; E_{ij}, G_{ij}, and L_{ij} denote the elastic modulus, shear modulus, and length of the ith limb's j^{th} member, respectively; A_{ij}, A_{ijy}, and A_{ijz} denote the area and the effective shear area of the cross-section along the y_{ij} and z_{ij} axes, respectively; I_{ijy} and I_{ijz} denote the area moment of cross-section inertia about the y_{ij} and z_{ij} axes, respectively. Finally, I_{ijp} denotes the polar moment of cross-section inertia.

The strain energy of the ith limb is as follows:

$$U_i = \sum_{j=1}^{c} U_{ij} = \frac{1}{2}\mathbf{W}_i^T \left(\sum_{j=1}^{c} \mathbf{C}_{ij} \right) \mathbf{W}_i = \frac{1}{2}\mathbf{W}_i^T \mathbf{C}_i \mathbf{W}_i \tag{9}$$

where $\mathbf{C}_i$ denotes the flexibility matrix of the ith limb corresponding to $\mathbf{W}_i$; c denotes the number of the member in the ith limb.

Elastic deformation $\boldsymbol{\Delta}_i$ of the ith limb corresponding to $\mathbf{W}_i$ is as follows according to Castigliano's second theorem:

$$\boldsymbol{\Delta}_i = \frac{\partial U_i}{\partial \mathbf{W}_i} = \mathbf{C}_i \mathbf{W}_i \tag{10}$$

The stiffness matrix of the ith limb constraint wrenches can be obtained as

$$\mathbf{K}_i = \mathbf{C}_i^{-1} \tag{11}$$

Equations (1), (2), (3) and (10) lead to

$$\mathbf{W}_i = \mathbf{K}_i \boldsymbol{\Delta}_i = \mathbf{K}_i \mathbf{J}_i^T \boldsymbol{\Delta}_o = \mathbf{K}_i \mathbf{J}_i^T \mathbf{C}_p \mathbf{W}_o = \mathbf{K}_i \mathbf{J}_i^T \mathbf{C}_p \mathbf{D}_{To} \mathbf{W}_T \tag{12}$$

Therefore, the strain energy of the ith limb's j^{th} member of parallel modules is as follows.

$$\begin{aligned}
U_{ij} &= \frac{1}{2}\mathbf{W}_i^{\text{T}} \boldsymbol{\Delta}_{ij} = \frac{1}{2}\mathbf{W}_i^{\text{T}} \mathbf{C}_{ij}\mathbf{W}_i = \frac{1}{2} \left(\mathbf{K}_i \mathbf{J}_i^{\text{T}} \mathbf{C}_p \mathbf{D}_{To} \mathbf{W}_T \right)^{\text{T}} \mathbf{C}_{ij} \left(\mathbf{K}_i \mathbf{J}_i^{\text{T}} \mathbf{C}_p \mathbf{D}_{To} \mathbf{W}_T \right) \\
&= \frac{1}{2}\mathbf{W}_T^{\text{T}} \left(\mathbf{D}_{To}^{\text{T}} \mathbf{C}_p^{\text{T}} \mathbf{J}_i \mathbf{K}_i^{\text{T}} \mathbf{C}_{ij} \mathbf{K}_i \mathbf{J}_i^{\text{T}} \mathbf{C}_p \mathbf{D}_{To} \right) \mathbf{W}_T = \frac{1}{2}\mathbf{W}_T^{\text{T}} \overline{\mathbf{C}}_{ij} \mathbf{W}_T
\end{aligned} \tag{13}$$

where $\overline{\mathbf{C}}_{ij}$ denotes the overall flexibility contribution matrix caused by the ith limb's j^{th} member of parallel modules for the hybrid robot.

The elastic deformation of the hybrid robot terminal caused by the ith limb's j^{th} member of parallel modules can be obtained based on the Castigliano's second theorem.

$$\overline{\boldsymbol{\Delta}}_{ij} = \frac{\partial U_{ij}}{\partial \mathbf{W}_T} = \overline{\mathbf{C}}_{ij} \mathbf{W}_T \tag{14}$$

Now, we have decoupled the elastic deformation of the hybrid robot end and the CCM caused by the ith limb's j^{th} member of parallel module of the hybrid robot through equation (14).

2.2. Elastic deformation of hybrid robot end caused by serial module

Elastic deformation $\mathbf{\Delta}_{si}$ of the jth member of serial module corresponding to $\mathbf{W}_T$ is as follows according to the strain energy and Castigliano's second theorem.

$$\mathbf{\Delta}_{sj} = \frac{\partial U_{sj}}{\partial \mathbf{W}_T} = \mathbf{C}_{sj}\mathbf{W}_T \tag{15}$$

where U_{sj} denotes the strain energy of jth member of the serial module; $\mathbf{C}_{sj}$ denotes the flexibility matrix corresponding to the $\mathbf{W}_T$ of the jth member of serial module.

The strain energy of the serial module U_s is as follows:

$$U_s = \sum_{j=1}^{g} U_{sj} = \frac{1}{2}\mathbf{W}_T^T \left(\sum_{j=1}^{g} \mathbf{C}_{sj} \right) \mathbf{W}_T = \frac{1}{2}\mathbf{W}_T^T\mathbf{C}_s\mathbf{W}_T \tag{16}$$

where $\mathbf{C}_s$ denotes the flexibility matrix of the serial module corresponding to $\mathbf{W}_T$; g denotes the number of members of the serial module.

The hybrid robot end elastic deformation caused by serial modules is as follows according to Castigliano's second theorem:

$$\mathbf{\Delta}_{Ts} = \frac{\partial U_s}{\partial \mathbf{W}_T} = \mathbf{C}_s\mathbf{W}_T \tag{17}$$

2.3. Elastic deformation of hybrid robot end

Finally, the elastic deformation of the hybrid robot terminal is equal to the sum of elastic deformation caused by parallel and serial modules according to the rigidity principle.

$$\mathbf{\Delta}_T = \mathbf{\Delta}_{Tp} + \mathbf{\Delta}_{Ts} = \mathbf{T}_{To}\mathbf{C}_p\mathbf{W}_o + \mathbf{C}_{Ts}\mathbf{W}_T = \left(\mathbf{T}_{To}\mathbf{C}_p\mathbf{D}_{To} + \mathbf{C}_{Ts} \right) \mathbf{W}_T = \mathbf{C}_H\mathbf{W}_T \tag{18}$$

where $\mathbf{\Delta}_T$ denotes the elastic deformation of the hybrid robot terminal; $\mathbf{C}_H$ denotes the overall flexibility of the hybrid robot corresponding to external screw $\mathbf{W}_T$.

Reference [21] decouples the contribution of each elastic element in the parallel module using the rigidity principle. In this approach, the contribution matrix of each elastic element to the stiffness of the mechanism becomes singular in some configurations, requiring the use of the generalized inverse operation to obtain the contribution of each elastic element to the end deformation of the mechanism. In contrast, in this paper, the parallel module operates entirely within the framework of strain energy and Castigliano's second theorem, which has a clear physical interpretation and avoids the occurrence of singularity issues that can arise when using the rigidity principle in parallel module.

3. Example 1: 3SPR + 1R hybrid mechanism

First, we employ a 3SPR + 1R hybrid mechanism to systematically describe our model, as illustrated in Fig. 4a. The parallel module consists of a mobile platform, a fixed platform, and three identical SPR branches. Each limb comprises an active prismatic joint (P), a passive spherical joint (S), and a passive revolute joint (R). These three limbs are evenly distributed at 120° intervals with respect to the connection points on the mobile platform (or fixed platform). The serial module is formed by an active revolute joint (R) and is connected to the hybrid module at the geometric center o of the mobile platform. The entire hybrid mechanism includes a total of four active joints, serving as inputs for the mechanism. The mobile platform and joints are assumed to be rigid. The elastic rods are made of structural steel, sharing the same cross-sectional area with a diameter of $d = 0.02$m. The elastic modulus is $E = 200$ GPa, and the Poisson's ratio is $\mu = 0.3$. $oA_1 = oA_2 = oA_3 = 0.13$m, $OB_1 = OB_2 = OB_3 = 0.18$m.

As shown in Fig. 4a, the parallel module's moving coordinate system $o\text{-}xyz$ has its origin o located at the geometric center of the mobile platform, the z-axis is perpendicular to the plane of the mobile platform, the x-axis is along the oA_1 direction, and the y-axis is determined by the right-hand rule. The
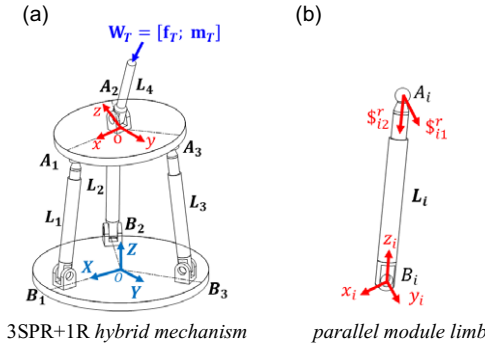
Figure 4. *Coordinate system of 3SPR + 1R hybrid mechanism.*

fixed coordinate system O-XYZ has its origin at the geometric center of the fixed platform, the Z-axis is vertically oriented upward, the X-axis is along the OB_1 direction, and the Y-axis is determined by the right-hand rule. As shown in Fig. 4b, the local coordinate system B_i-$x_iy_iz_i$ of the parallel module limb is depicted, the coordinate origin is located at point B_i, where the y_i-axis aligns with the direction of the revolute joint axis, and the z_i-axis aligns with the direction of the limb rod, pointing toward point A_i and the x_i-axis is determined by the right-hand rule.

Based on screw and reciprocal screw theory, the reciprocal dot product of the motion screw and the constraint force screw is zero [30].

$$\$_{ij} \circ \$^{r}_{ij} = 0 \tag{19}$$

When the active prismatic joint of the limb is locked, the motion screw system of the limb can be represented based on the local coordinate system B_i-$x_iy_iz_i$:

$$
\begin{aligned}
\$_{i1} &= \begin{bmatrix} 0 & 1 & 0 & 0 & 0 & 0 \end{bmatrix} \\
\$_{i2} &= \begin{bmatrix} 1 & 0 & 0 & 0 & L_i & 0 \end{bmatrix} \\
\$_{i3} &= \begin{bmatrix} 0 & 1 & 0 & -L_i & 0 & 0 \end{bmatrix} \\
\$_{i4} &= \begin{bmatrix} 0 & 0 & 1 & 0 & 0 & 0 \end{bmatrix}
\end{aligned}
\tag{20}
$$

where L_i represents the length of the limb rod.

According to equation (19), the constraint wrench system of the limb can be obtained as

$$
\begin{aligned}
\$^{r}_{i1} &= \begin{bmatrix} 0 & 1 & 0 & -L_i & 0 & 0 \end{bmatrix} \\
\$^{r}_{i2} &= \begin{bmatrix} 0 & 0 & 1 & 0 & 0 & 0 \end{bmatrix}
\end{aligned}
\tag{21}
$$

According to the physical significance of reciprocal screw, we know that when the active prismatic joint of the limb is locked, the limb imposes two constraint forces on the mobile platform at point A_i along the y_i and z_i axes, with magnitudes f_{i1} and f_{i2} (as shown in Fig. 4b). This can be expressed as $\mathbf{W}_i = [0, f_{i1}, f_{i2}, 0, 0, 0]^T = [\mathbf{f}_i, \mathbf{0}]^T$. In total, the three limbs collectively impose six constraint forces on the mobile platform. Therefore, the 3SPR + 1R hybrid mechanism is the underconstrained mechanism.

According to the knowledge of strain energy in material mechanics, the strain energy of limb can be expressed as

$$U_i = \frac{L_i}{2G_iA_i}f_{i1}^2 + \frac{L_i}{2E_iA_i}f_{i2}^2 + \frac{L_i^3}{6E_iI_{ix}}f_{i1}^2 \tag{22}$$

Table I. *Elastic deflection of the hybrid robot terminal.*

Method	Δ_{dx} (10^{-5}m)	Δ_{dy} (10^{-5}m)	Δ_{dz} (10^{-5}m)	Δ_{rx} (10^{-5}rad)	Δ_{ry} (10^{-5}rad)	Δ_{rz} (10^{-5}rad)
Analytical	2.916	0.828	0.452	23.124	-33.278	66.786
FEM	2.968	0.847	0.458	23.564	-33.978	67.632
Relative error (%)	1.78	2.32	1.44	1.90	2.10	1.27

According to equation (10), the flexibility matrix $\mathbf{C}_i$ of limb i is obtained as

$$\mathbf{C}_i = \begin{bmatrix} \dfrac{L_i}{G_i A_i} + \dfrac{L_i^3}{3E_i I_{ix}} & 0 \\ 0 & \dfrac{L_i}{E_i A_i} \end{bmatrix} \tag{23}$$

Stiffness matrix $\mathbf{K}_i$ and overall stiffness matrix $\mathbf{K}_p$ can be obtained by equations (6) and (11). The contribution of the parallel module to the elastic deformation of the hybrid robot end can be obtained by equation (5), where $\mathbf{J}_i = [\$_{i1}^r, \$_{i2}^r]$ represents the constrained screw system of limb i. The overall flexibility matrix corresponding to the serial module and $\mathbf{W}_T$, as well as the contribution to the elastic deformation of the hybrid mechanism end, can be obtained according to the equations (16) and (17). The elastic deformation of the hybrid mechanism end is obtained according to the equation (18) after solving the contribution of the parallel and serial modules to the elastic deformation of the hybrid mechanism end, respectively.

Validation is conducted using the finite element commercial software ANSYS software. In the ANSYS model, material and structural parameters are set based on those used in the theoretical model. The flexible limb rod is modeled using Beam 188 elements based on the Timoshenko beam theory, while the revolute joint and spherical joint are modeled using MPC184 elements in ANSYS. The configuration and structural parameters of the hybrid mechanism are as follows: When the active prismatic joint of the limb of the parallel module is locked, the length of limb rod is $L_1 = 0.25$m, $L_2 = L_3 = 0.3$m. The axis of the active revolute joint in the serial module is parallel to the x-axis of the moving coordinate o-xyz. When it is locked, the angle between the rod axis and the plane of the mobile platform is 60°, the length of the serial module rod is $L_4 = 0.2$m. Based on the fixed coordinate system O-XYZ, terminal external load is $\mathbf{W}_T = [20\text{N}, 30\text{N}, -50\text{N}, 30\text{N·m}, -30\text{N·m}, 40\text{N·m}]^T$. The comparative results of end deformation for the hybrid mechanism are listed in Table 1, with the maximum error of 2.32%. This validates the accuracy of the proposed model in this paper. The FEA simulation results of the hybrid mechanism are illustrated in Fig. 5.

4. Example 2: 4SRRR + 6R hybrid robot

4.1. Introduction of 4SRRR + 6R

The hybrid robot composed of a four-legged wall-climbing robot and serial robotic arms is developed based on the on-site work requirements of large and complex structural parts (Fig. 6). The parallel module (four-legged wall-climbing robot) consists of a moving platform, a fixed platform (the fixed foot and the working wall form a fixed platform when the four-legged wall climbing robot reaches the working position), and four identical SRRR limbs. The limb legs are symmetrical and are composed of three active rotating joints (R) and one passive ball hinge joint (S). The serial module (serial robotic arm) is composed of six active rotating joints (R), and the axes of the last three rotating joints intersect at one point. There are a total of 18 active rotating joints in the parallel and serial module as the input of the mechanism. The mobile platform and joints of hybrid robot are assumed to be rigid, and the elastic rod components are made of aluminum alloy 7075-T6, with their physical and structural parameters shown in Table 2.
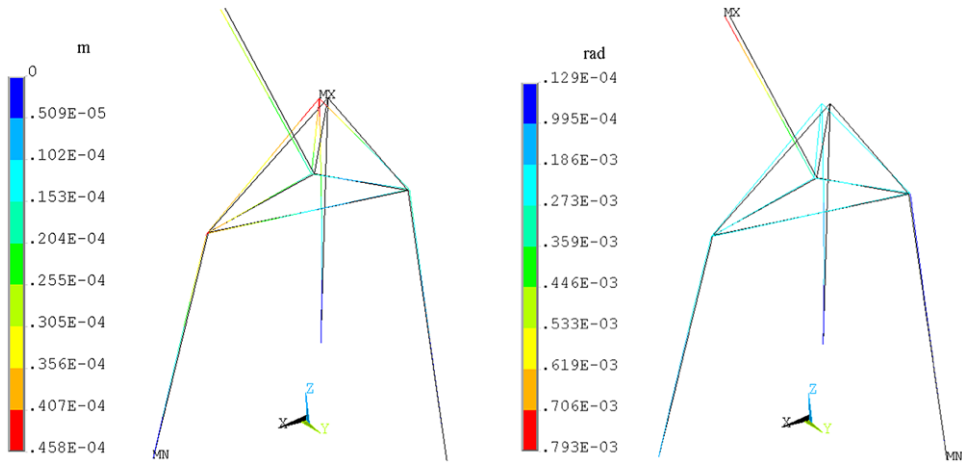
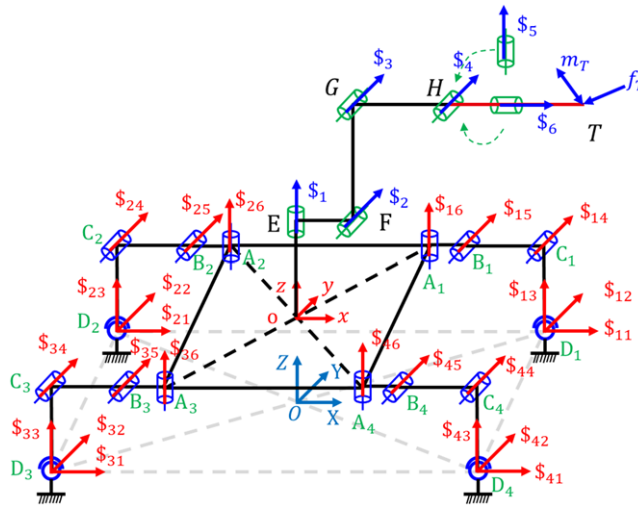**Figure 5.** *Contours of linear and angular displacement vectors.*

Figure 6. *4SRRR + 6R hybrid robot.*

The origin of parallel module moving coordinate system o-xyz is located at the geometric center of the moving platform; the z-axis is perpendicular to the plane where the moving platform is located; the x-axis is parallel to line A_3A_4; and the y-axis is determined by the right-hand rule. The origin of fixed coordinate system O-XYZ is located at the geometric center of the fixed platform. The Z-axis is vertically upward; the X-axis is parallel to the line of D_3D_4; and the Y-axis is determined by the right-hand rule.

The parallel module limb is connected to the moving platform through R-joint at A_i (the axis is perpendicular to the surface of the moving platform) and connected to the fixed platform through S-joint at D_i (Fig. 7a). $\mathbf{z}_{i1}$, $\mathbf{z}_{i2}$, and $\mathbf{z}_{i3}$ of the local coordinate systems A_i-$x_{i1}y_{i1}z_{i1}$, B_i-$x_{i2}y_{i2}z_{i2}$, and C_i-$x_{i3}y_{i3}z_{i3}$ are along the axis of A_i, B_i, and C_i, respectively. x_{i1}, x_{i2}, and x_{i3} point to the directions of A_iB_i, B_iC_i, and C_iD_i, respectively. The serial module establishes a coordinate system according to the DH method.

The foot must be perpendicular to the work surface due to the magnetic suction when the 4SRRR-6R hybrid robot is adsorbed on the work surface. Figure 8 illustrates the inverse kinematics calculation diagram of the limb of the 4SRRR-6R hybrid robot.

Table II. *Physical and structure parameter values of the 4SRRR + 6R hybrid robot.*

| Parameters		Units	Values
E	Elastic modulus of aluminum alloy	Pa	7.1E10
μ	Poisson's ratio of aluminum alloy		0.33
L_A	The length of links A_2A_3 and A_4A_1	m	0.54
W_A	The length of links A_1A_2 and A_3A_4	m	0.54
L_{p1}	The length of link A_iB_i ($i = 1,2,3$, and 4)	m	0.140
L_{p2}	The length of link B_iC_i ($i = 1,2,3$, and 4)	m	0.350
L_{p3}	The length of link C_iD_i ($i = 1,2,3$, and 4)	m	0.350
d_{p1}/D_{p1}	The inner diameter of link A_iB_i ($i = 1,2,3$, and4)	m	0.054/0.070
d_{p2}/D_{p2}	The inner diameter of link B_iC_i ($i = 1,2,3$, and 4)	m	0.054/0.070
d_{p3}/D_{p3}	The inner diameter of link C_iD_i ($i = 1,2,3$, and 4)	m	0.054/0.070
L_{s1}	The length of link oE	m	0.250
L_{s2}	The length of link EF	m	0.050
L_{s3}	The length of link FG	m	0.350
L_{s4}	The length of link GH	m	0.350
L_{s5}	The length of link HT	m	0.100
d_{s1}/D_{s1}	The inner and outer diameter of link oE	m	0.150/0.180
d_{s2}/D_{s2}	The inner and outer diameter of link EF	m	0.130/0.150
d_{s3}/D_{s3}	The inner and outer diameter of link FG	m	0.110/0.130
d_{s4}/D_{s4}	The inner and outer diameter of link GH	m	0.090/0.110
d_{s5}/D_{s5}	The inner and outer diameter of link HT	m	0.090/0.110
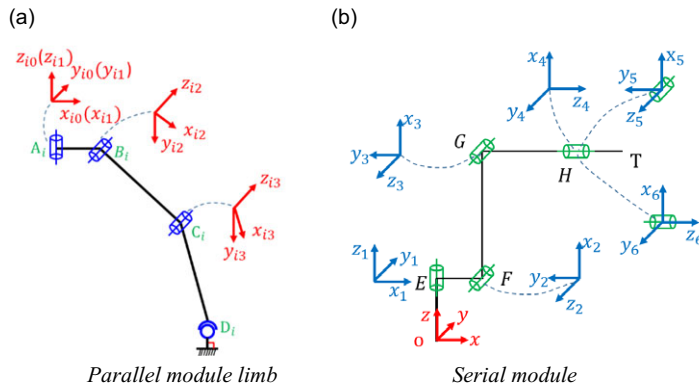
Figure 7. *Coordinate system of parallel module limb and serial module.*

The coordinate of A_i in the moving coordinate system is $({}^ox_{Ai}, {}^oy_{Ai}, {}^oz_{Ai})$, and the coordinates of D_i are $({}^ox_{Di}, {}^oy_{Di}, {}^oz_{Di})$. The following equation according to the geometric relationships is

$$\begin{cases} \eta_{i1} = atan2 \left({}^oy_{Di} - {}^oy_{Ai}, \ {}^ox_{Di} - {}^ox_{Ai}\right) \\ L_{AiDi} = abs \left[\left({}^ox_{Di} - {}^ox_{Ai}\right) / \cos\left(\eta_{i1}\right)\right] \\ H_i = abs \left({}^oz_{Ai} - {}^oz_{Di}\right) \\ L_{BiDi} = \sqrt{\left(L_{AiDi} - L_1\right)^2 + H_i^2} \end{cases} \tag{24}$$
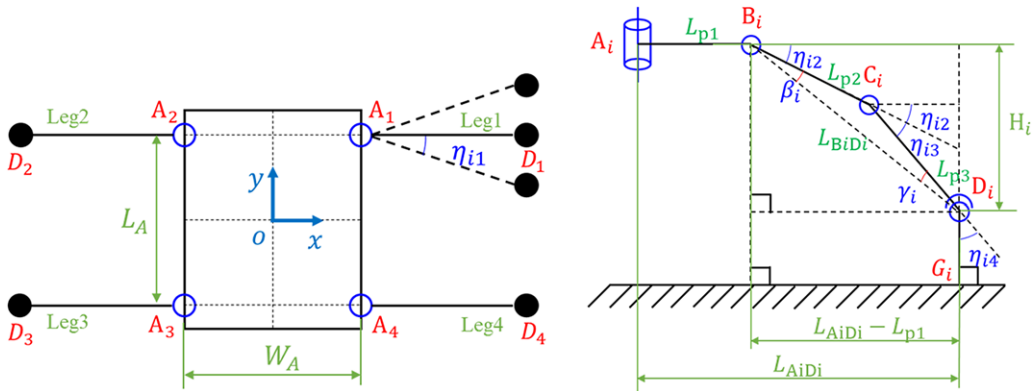
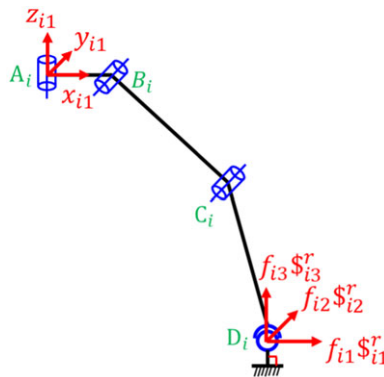**Figure 8.** *Inverse kinematics of 4SRRR wall climbing robot.*

Figure 9. *Constraint wrench system applied by the ith limb on the moving platform.*

According to the cosine theorem,

$$\begin{cases} \eta_{3i} = \pi - acos\left(\dfrac{L_2^2 + L_3^2 - L_{BiDi}^2}{2L_2L_3}\right) \\ \beta_i = acos\left(\dfrac{L_2^2 + L_{BiDi}^2 - L_3^2}{2L_2L_{BiDi}}\right) \end{cases} \tag{25}$$

Then,

$$\eta_{i2} + \beta_i = atan2\,(H_i, L_i - L_1) \tag{26}$$

We can obtain

$$\begin{cases} \eta_{i2} = atan2\,(H_i, L_i - L_1) - \beta_i \\ \eta_{i4} = \dfrac{\pi}{2} - \eta_{i2} - \eta_{i3} \end{cases} \tag{27}$$

4.2. Static stiffness modeling of hybrid robots

Figure 9 shows the constraint wrench system imposed by the limb on the mobile platform. Utilizing the screw and reciprocal screw theory, the constraint wrench system of the limb can be obtained based on local coordinate systems A_i-$x_{i1}y_{i1}z_{i1}$:
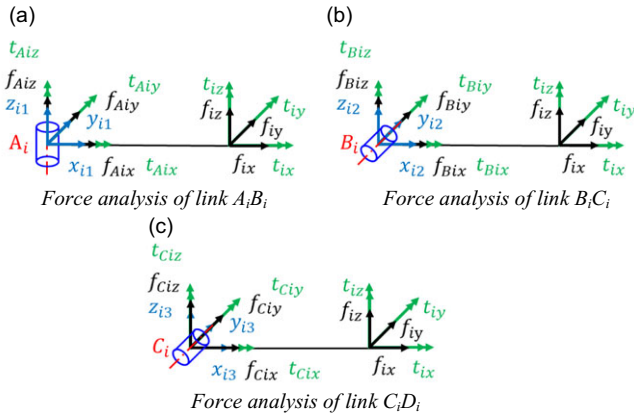
(a)

Force analysis of link A_iB_i

(b)

Force analysis of link B_iC_i

(c)

Force analysis of link C_iD_i

Figure 10. *Force analysis of each component of the limb.*

$$\$_{i1}^r = \begin{bmatrix} 1 & 0 & 0 & 0 & z_{Di} & -y_{Di} \end{bmatrix}$$
$$\$_{i1}^r = \begin{bmatrix} 0 & 1 & 0 & -z_{Di} & 0 & x_{Di} \end{bmatrix} \tag{28}$$
$$\$_{i1}^r = \begin{bmatrix} 0 & 0 & 1 & y_{Di} & -x_{Di} & 0 \end{bmatrix}$$

The limb leg exerts three constraint forces along the x_{i1}, y_{i1}, and z_{i1} axes on the robot mobile platform at point D_i when the three active joints of the limb leg are all locked according to screw and reciprocal screw theory. The amplitudes are f_{i1}, f_{i2}, and f_{i3} (Fig. 9), that is, $\mathbf{W}_i = [f_{i1} f_{i2} f_{i3} \, 0 \, 0 \, 0]^T = [\mathbf{f}_i \, \mathbf{0}]^T$. The four limb legs exert 12 constraint force on the robot's moving platform. The solving requires simultaneous equations involving additional supplementary equations and static equilibrium equations. Therefore, the four-legged climbing robot is the overconstrained mechanism.

The force screw acting on the A_i point can be expressed as follows under branch coordinate system A_i-$x_{i1}y_{i1}z_{i1}$ according to the translation principle of force in theoretical mechanics:

$$\mathbf{W}_{Ai} = [\mathbf{f}_{Ai}; \mathbf{t}_{Ai}] \tag{29}$$

where $\mathbf{f}_{Ai}$ represents the force at point A_i, and $\mathbf{f}_{Ai} = \mathbf{f}_i$; $\mathbf{t}_{Ai}$ represents the torque at point A_i, and $\mathbf{t}_{Ai} = \mathbf{A}_i\mathbf{D}_i \times \mathbf{f}_i$.

Figure 10a, 10b and 10c illustrate the force analysis of the A_iB_i, B_iC_i and C_iD_i rods within their respective branches based on the strain energy in material mechanics, and the strain energy of the A_iB_i, B_iC_i and C_iD_i rod in Branch i can be expressed as

$$U_{ik} = a_{ik1}f_{i1}^2 + a_{ik2}f_{i2}^2 + a_{ik3}f_{i3}^2 + a_{ik4}f_{i1}f_{i2} + a_{ik5}f_{i2}f_{i3} + a_{ik6}f_{i3}f_{i1} \tag{30}$$

where a_{ik1}, a_{ik2}, …, and a_{ik6} ($k = 1,2,3$) are the coefficients obtained based on the equation with $\mathbf{W}_i$ as the variable. C_{i1} can be solved according to the equation.

The strain energy of the ith limb is equal to the sum of the strain energy of each member.

$$U_i = U_{i1} + U_{i2} + U_{i3} = a_{i1}f_{i1}^2 + a_{i2}f_{i2}^2 + a_{i3}f_{i3}^2 + a_{i4}f_{i1}f_{i2} + a_{i5}f_{i2}f_{i3} + a_{i6}f_{i3}f_{i1} \tag{31}$$

where $a_{ij} = a_{i1j} + a_{i2j} + a_{i3j}$ ($j = 1, 2, …, 6$).

The elastic deformation of the end of limb i along the axis of the constrained screw is as follows according to equation (7).

$$\Delta_{i1} = \frac{\partial U_i}{\partial f_{i1}} = 2a_{i1}f_{i1} + a_{i4}f_{i2} + a_{i6}f_{i3}$$

$$\Delta_{i2} = \frac{\partial U_i}{\partial f_{i2}} = a_{i4}f_{i1} + 2a_{i2}f_{i2} + a_{i5}f_{i3} \qquad (32)$$

$$\Delta_{i3} = \frac{\partial U_i}{\partial f_{i3}} = a_{i6}f_{i1} + a_{i5}f_{i2} + 2a_{i3}f_{i3}$$

The flexibility matrix of limb i can be obtained as

$$\mathbf{C}_i = \begin{bmatrix} 2a_{i1} & a_{i4} & a_{i6} \\ a_{i4} & 2a_{i2} & a_{i5} \\ a_{i6} & a_{i5} & 2a_{i3} \end{bmatrix} \qquad (33)$$

Stiffness matrix $\mathbf{K}_i$ and overall stiffness matrix $\mathbf{K}_p$ can be obtained by equations (6) and (11). The contribution of the parallel module to the elastic deformation of the hybrid robot end can be obtained by equation (5), and the contribution of each member of the parallel module to the elastic deformation of the hybrid robot end can be obtained by equation (14), where $\mathbf{J}_i = [\$_{i1}^r, \$_{i2}^r, \$_{i3}^r]$ represents the constrained screw system of limb i.

The decoupling flexibility matrix corresponding to serial module rod j and $\mathbf{W}_T$, as well as the contribution to the elastic deformation of the hybrid robot end, can be obtained according to the equation (15). The overall flexibility matrix corresponding to the serial module and $\mathbf{W}_T$, as well as the contribution to the elastic deformation of the hybrid robot end, can be obtained according to the equations (16) and (17).

The elastic deformation of the hybrid robot end is obtained according to the equation (18) after solving the contribution of the parallel and serial modules to the elastic deformation of the hybrid robot end, respectively.

4.3. Comparison between the analytical model and finite element model

The finite element commercial software ANSYS was used to verify the correctness and feasibility of the proposed method in the work. The material and structural parameters are given based on the parameters used in the theoretical model in the ANSYS model. The flexible limb is modeled using Beam 188 units based on the theory of Timoshenko.

Two typical working conditions of mobile welding are considered. Working pose 1: Four-legged wall-climbing robot (parallel module) limbs: $\theta_{i1} = 0°$, $\theta_{i2} = 10°$, and $\theta_{i3} = 70°$ ($i = 1, 2, 3, 4$). Serial module: joint angle $\theta_{s1} = 90°$, $\theta_{s2} = -45°$, $\theta_{s3} = 0°$, $\theta_{s4} = 0°$, $\theta_{s5} = -50°$, and $\theta_{s6} = 0$. Working pose 2: Four-legged wall-climbing robot (parallel module) limbs: $\theta_{i1} = 45°$, $\theta_{i2} = 10°$, and $\theta_{i3} = 70°$ ($i = 1, 2, 3, 4$). Serial module: joint angle $\theta_{s1} = 120°$, $\theta_{s2} = -45°$, $\theta_{s3} = 0°$, $\theta_{s4} = 0°$, $\theta_{s5} = -50°$, and $\theta_{s6} = 0°$. Terminal external load $\mathbf{W}_T = [50\text{N}, 80\text{N}, -100\text{N}, 0, 0, 0]^T$.

Table 3 lists the comparison of tool terminal deformation results of the hybrid robot between the proposed analytical model and the finite element model (FEM), where the maximum error is 2.35%. The discrepancies between the theoretical model and the FEM mainly arise from differences in mesh partitioning and calculation errors. The correctness and accuracy of the proposed model are verified. Figure 11 shows the FEM results of the two poses of the hybrid robot.

4.4. Stiffness performance evaluation

The linear and angular displacements generated when the terminal of the hybrid robot works along the specified trajectory are used to evaluate the stiffness performance of the robot.

Table III. *Elastic deflection of the hybrid robot terminal.*

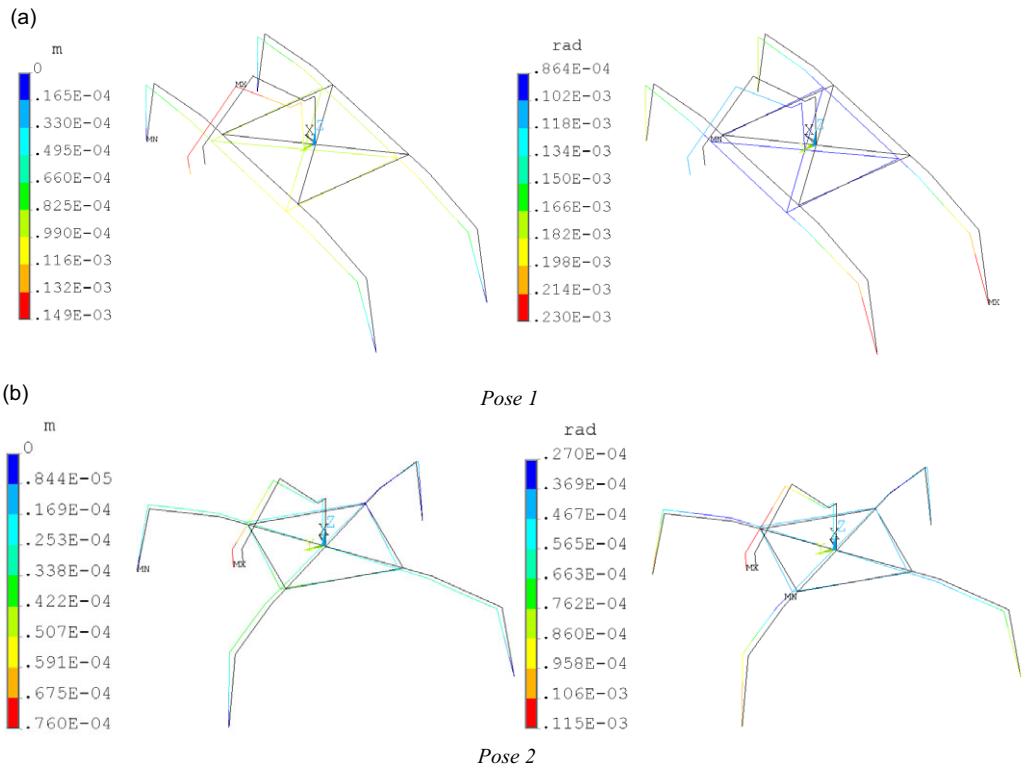| Pose	Method	Δ_{dx} (10^{-5}m)	Δ_{dy} (10^{-5}m)	Δ_{dz} (10^{-5}m)	Δ_{rx} (10^{-5}rad)	Δ_{ry} (10^{-5}rad)	Δ_{rz} (10^{-5}rad)
1	Analytical	3.339	10.520	−6.126	−9.710	−3.358	−4.485
	FEM	3.411	10.740	−6.268	−9.842	−3.415	−4.566
	Relative error (%)	2.11	2.06	2.26	1.34	1.68	1.77
2	Analytical	6.029	3.241	−2.931	−1.181	−7.359	−8.618
	FEM	6.157	3.312	−3.001	−1.193	−7.459	−8.746
	Relative error (%)	2.07	2.14	2.35	0.97	1.34	1.46

(a)

Pose 1

(b)

Pose 2

Figure 11. *Contours of linear and angular displacement vectors.*

$$\begin{cases} \Delta_d = \sqrt{\Delta_{dx}^2 + \Delta_{dy}^2 + \Delta_{dz}^2} \\ \Delta_r = \sqrt{\Delta_{rx}^2 + \Delta_{ry}^2 + \Delta_{rz}^2} \end{cases} \tag{34}$$

The robot performs welding or polishing work along a specified trajectory. The four-legged wall-climbing robot (parallel module) limbs: $\theta_{i1} = 45°$, $\theta_{i2} = 10°$, and $\theta_{i3} = 70°$ ($i = 1, 2, 3, 4$). The terminal tool of the robot works along the path of the sinusoidal curve ($x = -0.3:0.02:0.3$, $y = 0.005\sin(8\pi x) + 0.5$, and $z = 0.1$) in a specific posture, and the external load is $\mathbf{W}_T = [50\text{N}, 80\text{N}, -100\text{N}, 0, 0, 0]^T$. The linear and angular displacement reach their maximum values at the same time, which are 8.551e-5 m and 1.243e-4 rad, respectively, when the robot end is close to $(-0.3\,\text{m}, 0.495\,\text{m}, 0.1\,\text{m})$ (Fig. 12).

(a)   *(b)*

Linear deflection   *Angular deflection*
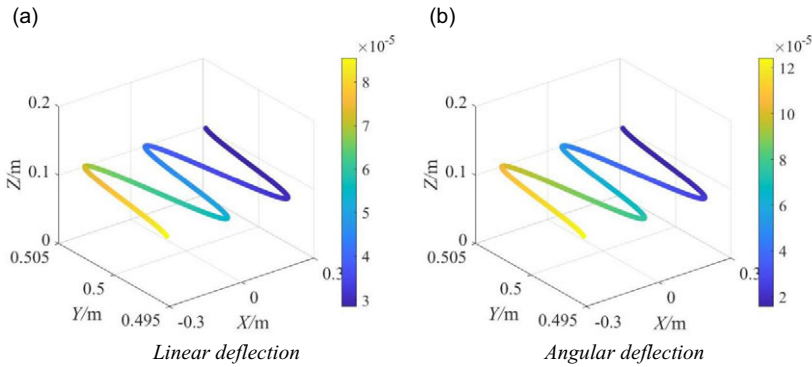
Figure 12. *Linear and angular deflections of the hybrid robot terminal in the prescribed trajectory.*

The contribution of each elastic element to the elastic deformation of the hybrid robot end is expressed by the equation as follows when the robot works along the specified trajectory.

$$
\begin{cases}
\overline{\Delta}_{ijd} = \dfrac{\sum \Delta_{ijd}}{N} \\[3mm]
\overline{\Delta}_{ijr} = \dfrac{\sum \Delta_{ijr}}{N}
\end{cases}
\tag{35}
$$

where Δ_{ijd} and Δ_{ijr} represent the linear and angular displacement of the elastic deformation of the robot end caused by the elastic deformation of limb i's member j, respectively; $\overline{\Delta}_{ijd}$ and $\overline{\Delta}_{ijr}$ represent the average values of the linear and angular displacement caused by the elastic deformation of limb i's member j when the hybrid robot end is working along a specified trajectory. N represents the number of discrete points in the work trajectory.

The average linear displacement of the hybrid robot end is 5.037×10^{-5}m when it works along the sinusoidal curve path mentioned above (Fig. 12a). Table 4 shows the average linear displacement of each elastic element (the linear displacement along the x-, y-, and z-axes directions can be listed separately if necessary). The linear displacement at the tool end of the hybrid robot is mainly caused by the serial robot arm rod FG, followed by rods B_1C_1, oE, and GH. Therefore, the serial robotic arm rod FG should be improved first to improve the linear stiffness of the hybrid robot.

The following five situations are considered to quantitatively evaluate the effect of improving the stiffness performance of each elastic element on the stiffness of the terminal line of the hybrid robot: (1) use the original physical parameters (Table 2), (2) the outer diameter of the FG of the serial robotic arm rod is increased by 20%, and the remaining parameters remain unchanged, (3) the outer diameter of parallel-module rod B_1C_1 is increased by 20%, and the remaining parameters remain unchanged, (4) the outer diameter of the oE of the serial robotic arm rod is increased by 20%, and the remaining parameters remain unchanged, and (5) the outer diameter of the GH of the serial robotic arm rod is increased by 20%, and the remaining parameters remain unchanged.

Table 5 lists the influence of the above five conditions on the linear displacement of the terminal of the hybrid robot working along the specified trajectory. The linear displacement in working conditions (2)–(5) is reduced by 12.71%, 9.61%, 7.27%, and 6.06%, respectively, compared with that in working conditions (1). Improving the FG stiffness performance of the serial robotic arm rod can most improve the linear stiffness of the hybrid robot. In other words, the method proposed in this paper allows for effective control of the stiffness performance of the robot when the external wrench is known. This enables the maximization of robot stiffness performance or lightweight design. However, a limitation of this method is that it cannot pinpoint the components that have the greatest impact on the robot's stiffness performance when the external wrench is unknown.

Table IV. *Average linear elastic deflection contribution of each component of the 4SRRR + 6R.*

$\overline{\Delta}_{11d}$	$\overline{\Delta}_{12d}$	$\overline{\Delta}_{13d}$	$\overline{\Delta}_{21d}$	$\overline{\Delta}_{22d}$	$\overline{\Delta}_{23d}$	$\overline{\Delta}_{31d}$	$\overline{\Delta}_{32d}$	$\overline{\Delta}_{33d}$
4.740e-6	6.605e-6	5.002e-6	4.942e-6	4.325e-6	2.094e-6	8.399e-7	3.579e-6	2.083e-6
$\overline{\Delta}_{41d}$	$\overline{\Delta}_{42d}$	$\overline{\Delta}_{43d}$	$\overline{\Delta}_{s1d}$	$\overline{\Delta}_{s2d}$	$\overline{\Delta}_{s3d}$	$\overline{\Delta}_{s4d}$	$\overline{\Delta}_{s5d}$	
5.469e-7	1.183e-6	4.529e-7	6.272e-6	1.702e-6	1.060e-5	6.001e-6	9.636e-7	

Note: $\overline{\Delta}_{ijd}$ and $\overline{\Delta}_{sjd}$ denote the average linear elastic deflection contribution of the ith limb's j^{th} member of parallel modules and the jth member of serial module, respectively, its unit is m.

Table V. *Comparison of the effects of each elastic component on the resulting linear deflection of the 4SRRR + 6R.*

	Case 1	Case 2	Case 3	Case 4	Case 5
$\overline{\Delta}_d$/m	5.037e-5	4.397e-5	4.553e-5	4.671e-5	4.732e-5
Change (%)	/	12.71	9.61	7.27	6.06

Table VI. *Average angular elastic deflection contribution of each component of the 4SRRR + 6R.*

$\overline{\Delta}_{11r}$	$\overline{\Delta}_{12r}$	$\overline{\Delta}_{13r}$	$\overline{\Delta}_{21r}$	$\overline{\Delta}_{22r}$	$\overline{\Delta}_{23r}$	$\overline{\Delta}_{31r}$	$\overline{\Delta}_{32r}$	$\overline{\Delta}_{33r}$
6.498e-6	4.385e-6	9.966e-7	7.517e-6	5.932e-6	1.039e-6	2.076e-6	2.564e-6	4.436e-7
$\overline{\Delta}_{41r}$	$\overline{\Delta}_{42r}$	$\overline{\Delta}_{43r}$	$\overline{\Delta}_{s1r}$	$\overline{\Delta}_{s2r}$	$\overline{\Delta}_{s3r}$	$\overline{\Delta}_{s4r}$	$\overline{\Delta}_{s5r}$	
1.574e-6	1.407e-6	1.922e-7	1.064e-5	3.134e-6	2.271e-5	2.041e-5	5.410e-6	

Note: $\overline{\Delta}_{ijr}$ and $\overline{\Delta}_{sjr}$ denote the average angular elastic deflection contribution of the ith limb's j^{th} member of parallel modules and the jth member of serial module, respectively, its unit is rad.

Table VII. *Comparison of the effects of each elastic component on the resulting angular deflection of the 4SRRR + 6R.*

	Case 1	Case 2	Case 3	Case 4	Case 5
$\overline{\Delta}_r$/rad	6.382e-5	4.870e-5	5.880e-5	6.046e-5	6.132e-5
change (%)	/	23.69	7.87	5.26	3.92

Similarly, the average angular displacement of the hybrid robot end when working along the sinusoidal curve path is 6.382×10^{-5} m (Fig. 12b). Table 6 shows the angular displacement of each elastic element (the angular displacement generated around the x-, y-, and z-axes can be listed separately if necessary). The angular displacement of the tool terminal of the hybrid robot is mainly caused by serial robot arm rod FG, followed by rod GH, oE, and A_2B_2. Therefore, serial robotic arm rod FG should be improved first to improve the terminal line stiffness of the hybrid robot.

The following five situations are considered to quantitatively evaluate the influence of each elastic element on the stiffness of the terminal angular of the hybrid robot: (1) use the original physical parameters (Table 2), (2) the outer diameter of the FG of the serial robotic arm rod is increased by 20%, and the remaining parameters remain unchanged, (3) the outer diameter of the parallel module rod GH increased by 20%, and the remaining parameters remained unchanged, (4) the outer diameter of the oE of the serial robotic arm rod is increased by 20%, and the remaining parameters remain unchanged, and (5) the outer diameter of the serial robotic arm rod A_2B_2 increased by 20%, and the remaining parameters remained unchanged.

Table 7 shows the influence of the above five conditions on the angular displacement of the terminal of the hybrid robot working along the specified trajectory. The angular displacements of cases (2)–(5)

are reduced by 23.69%, 7.87%, 5.26%, and 3.92%, respectively, compared with case (1). Improving the *FG* stiffness performance of the serial robotic arm rod can most improve the linear stiffness of the hybrid robot.[1]

5. Conclusions

The decoupling method of the elastostatic stiffness model of hybrid robots is proposed in the work based on the rigidity principle, screw theory, strain energy, and Castigliano's second theorem. The contribution of each elastic component to the stiffness performance of the robot is decoupled. This method decoupled the overall CCM of each elastic element to the robot based on the strain energy method, which avoided the singularity problem of that based on the rigidity principle.

This paper first introduces the model principles using a 3SPR hybrid mechanism and then applies them to a hybrid robot (4SRRR + 6R). The 4SRRR + 6R hybrid robot is composed of a four-legged wall-climbing robot and serial robotic arm. when the terminal of the robot tool is working along a specified trajectory, the rod *FG* has the greatest impact on the linear and angular displacement of the robot end. For the linear (angular) displacement, it is followed by the rod B_1C_1, *oE*, *GH* (the rod *GH*, *oE*, A_2B_2). Five situations are considered for linear (angular) displacement to verify the feasibility of the model proposed in the work: (1) In case 1, we use the original physical parameters; (2) In case 2, the outer diameter of the rod *FG* (*FG*) was increased by 20%. (3)In case 3, the outer diameter of the rod B_1C_1 (*GH*) was increased by 20%. (4) In case 4, the outer diameter of the rod *oE* (*oE*) is increased by 20%. (5) In case 5, the outer diameter of the rod *GH* (A_2B_2) is increased by 20%. As compared to case 1, the resulting linear (angular) deflections of case 2-5 are reduced by 12.71%, 9.61%, 7.27%, and 6.06% (23.69%, 7.87%, 5.26%, and 3.92%), respectively.

In conclusion, selectively improving the stiffness performance of a single elastic element can improve the overall linear and angular stiffness of the robot. It should be noted that if the improvement of linear stiffness and angular stiffness performance does not involve the same component, we need to make targeted choices based on engineering requirements. If the focus is more on linear stiffness performance, we can choose to enhance components that have a significant impact on linear stiffness. Alternatively, design personnel can skillfully balance between the two by assigning appropriate weight factors to components that significantly enhance both linear and angular stiffness based on experience. This enables a judicious distribution of quality. The model proposed in the work decoupled the contribution of each elastic element to the terminal linear and angular stiffness of the hybrid robot. The model has physical significance and provides a new way to improve the linear and angular stiffness of the hybrid robot.

---

[1]The finite element simulation validation of the influence of a single member on the overall stiffness, based on the variation in the stiffness of a single member, can be found in the Link: https://pan.baidu.com/s/1oGDH4S42wEiOiqw4hpyGvw?pwd=6666.

References

[1] J. Wu, T. Li, J. Wang and L. Wang, "Stiffness and natural frequency of a 3-DOF parallel manipulator with consideration of additional leg candidates," *Robot Auton Syst* **61**(8), 868–875 (2013).

[2] J. Wu, H. Ye, G. Yu and T. Huang, "A novel dynamic evaluation method and its application to a 4-DOF parallel manipulator," *Mech Mach Theory* **168**, 104627 (2022).

[3] J. Wu, Y. Gao, B. Zhang and L. Wang, "Workspace and dynamic performance evaluation of the parallel manipulators in a spray-painting equipment," *Robot Comp-Integ Manuf* **44**, 199–207 (2017).

[4] J. Zhang, Y. Zhao and Y. Jin, "Kinetostatic-model-based stiffness analysis of exechon PKM," *Robot Comp-Integr Manuf* **37**, 208–220 (2016).

[5] H. P. Shen, Z. Q. Zhu and Q. M. Meng, "Kinematics and stiffness modeling analysis of spatial 2T1R parallel mechanism with zero coupling degree," *Trans Chin Soc Ag Mach* **51**(10), 411–420 (2020).

[6] H. S. Kim and H. Lipkin, "Stiffness of parallel manipulators with serially connected legs," *J Mech Robot* **6**(3), 031001 (2014).

[7] A. Pashkevich, A. Klimchik and D. Chablat, "Enhanced stiffness modeling of manipulators with passive joints," *Mech Mach Theory* **46**(5), 662–679 (2011).

[8] A. Taghvaeipour, J. Angeles and L. Lessard, "On the elastostatic analysis of mechanical systems," *Mech Mach Theory* **58**(3), 202–216 (2012).

[9] Z. Huang, Y. Zhao and J. F. Liu, "Kinetostatic analysis of 4-R(CRR) parallel manipulator with overconstraints via reciprocal-screw theory," *Adv Mech Eng* **2**, 404960 (2010).

[10] B. Hu, "Kinematically identical manipulators for the exechon parallel manipulator and their comparison study," *Mech Mach Theory* **103**, 117–137 (2016).

[11] S.-C. Wang, H. Hikita, H. Kubo, Y.-S. Zhao, Z. Huang and T. Ifukube, "Kinematics and dynamics of a 6 degree-of-freedom fully parallel manipulator with elastic joints," *Mech Mach Theory* **38**(5), 439–461 (2003).

[12] Y. Xu, J. Yao and Y. Zhao, "Inverse dynamics and internal forces of the redundantly actuated parallel manipulators," *Mech Mach Theory* **51**, 172–184 (2012).

[13] Y. Lu, L. Chen, P. Wang, B. Zhang, Y. S. Zhao and B. Hu, "Statics and stiffness analysis of a novel six-component force/torque sensor with 3-RPPS compliant parallel structure," *Mech Mach Theory* **62**, 99–111 (2013).

[14] Y. Xu, W. Liu, J. Yao and Y. Zhao, "A method for force analysis of the overconstrained lower mobility parallel mechanism," *Mech Mach Theory* **88**, 31–48 (2015).

[15] J. Enferadi and A. A. Tootoonchi, "Accuracy and stiffness analysis of a 3-RRP spherical parallel manipulator," *Robotica* **29**(2), 193–209 (2011).

[16] A. Rezaei, A. Akbarzadeh and M.-R. Akbarzadeh-T., "An investigation on stiffness of a 3-PSP spatial parallel mechanism with flexible moving platform using invariant form," *Mech Mach Theory* **51**, 195–216 (2012).

[17] A. Rezaei and A. Akbarzadeh, "Position and stiffness analysis of a new asymmetric 2PRRPPR parallel CNC machine," *Adv Robot* **27**(2), 133–145 (2013).

[18] S. J. Yan, S. K. Ong and A. Y. C. Nee, "Stiffness analysis of parallelogram-type parallel manipulators using a strain energy method," *Robot Comp-Int Manuf* **37**, 13–22 (2016).

[19] C. Y. Q. C. Li, Q. H. Chen and L. M. Xu, "Elastostatic stiffness modeling of overconstrained parallel manipulators," *Mech Mach Theory* **112**, 58–74 (2018).

[20] C. Yang, Q. Chen, J. Tong and Q. Li, "Elastostatic stiffness analysis of a 2PUR-PSR overconstrained parallel mechanism," *Int J Precis Eng Manuf* **20**(4), 569–581 (2019).

[21] C. Yang, Q. Li and Q. Chen, "Decoupled elastostatic stiffness modeling of parallel manipulators based on the rigidity principle," *Mech Mach Theory* **145**, 103718 (2020).

[22] A. Klimchik, A. Pashkevich and D. Chablat, "Fundamentals of manipulator stiffness modeling using matrix structural analysis," *Mech Mach Theory* **133**, 365–394 (2019).

[23] A. Klimchik, D. Chablat and A. Pashkevich, "Stiffness modeling for perfect and non-perfect parallel manipulators under internal and external loadings," *Mech Mach Theory* **79**, 1–28 (2014).

[24] C. Zhao, H. Guo, D. Zhang, R. Liu, B. Li and Z. Deng, "Stiffness modeling of n(3RRlS) reconfigurable series-parallel manipulators by combining virtual joint method and matrix structural analysis," *Mech Mach Theory* **152**, 103960 (2020).

[25] G. Yu, J. Wu and L. Wang, "Stiffness model of a 3-DOF parallel manipulator with two additional legs," *Int J Adv Robot Syst* **11**(10), 173 (2014).

[26] A. Cammarata, "Unified formulation for the stiffness analysis of spatial mechanisms," *Mech Mach Theory* **105**, 272–284 (2016).

[27] A. Cammarata, D. Condorelli and R. Sinatra, "An algorithm to study the elastodynamics of parallel kinematic machines with lower kinematic pairs," *J Mech Robot* **5**(1), 011004 (2012).

[28] J. Wu, J. Wang, L. Wang, T. Li and Z. You, "Study on the stiffness of a 5-DOF hybrid machine tool with actuation redundancy," *Mech Mach Theory* **44**(2), 289–305 (2009).

[29] D. Deblaise, X. Hernot and P. Maurine, "A Systematic Analytical Method for PKM Stiffness Matrix Calculation," **In:** *IEEE International Conference on Robotics & Automation*, (2006) pp. 4213–4219.

[30] R. A. Ball. *Treatise on the Theory of Screws* (Cambridge University Press, England, 1900). pp. 1–30.